Bandgap Engineering of Phosphorene by Laser Oxidation toward Functional 2D Materials

Junpeng Lu,[†,#] Jing Wu,[†,#] Alexandra Carvalho,[‡,#] Angelo Ziletti,[§] Hongwei Liu,[∥] Junyou Tan,[‡] Yifan Chen,[∥] A. H. Castro Neto,[†,‡] Barbaros Özyilmaz,[*,†,‡] and Chorng Haur Sow[*,†,‡]

[†]Department of Physics, National University of Singapore, 2 Science Drive 3, Singapore 117542, Singapore, [‡]Center For Advanced 2D Materials and Graphene Research Center, National University of Singapore, 6 Science Drive 2, Singapore 117546, Singapore, [§]Department of Chemistry, Boston University, 590 Commonwealth Avenue, Boston, Massachusetts 02215, United States, and [∥]Institute of Materials Research and Engineering, A*STAR (Agency for Science, Technology and Research), 3 Research Link, Singapore 117602, Singapore. [#]These authors contributed equally to this work.

ABSTRACT We demonstrate a straightforward and effective laser pruning approach to reduce multilayer black phosphorus (BP) to few-layer BP under ambient condition. Phosphorene oxides and suboxides are formed and the degree of laser-induced oxidation is controlled by the laser power. Since the band gaps of the phosphorene suboxide depend on the oxygen concentration, this simple technique is able to realize localized band gap engineering of the thin BP. Micropatterns of few-layer phosphorene suboxide flakes with unique optical and fluorescence properties are created. Remarkably, some of these suboxide flakes display long-term (up to 2 weeks) stability in ambient condition. Comparing against the optical properties predicted by first-principle calculations, we develop a "calibration" map in using focused laser power as a handle to tune the band gap of the BP suboxide flake. Moreover, the surface of the laser patterned region is altered to be sensitive to toxic gas by way of fluorescence contrast. Therefore, the multicolored display is further demonstrated as a toxic gas monitor. In addition, the BP suboxide flake is demonstrated to exhibit higher drain current modulation and mobility comparable to that of the pristine BP in the electronic application.

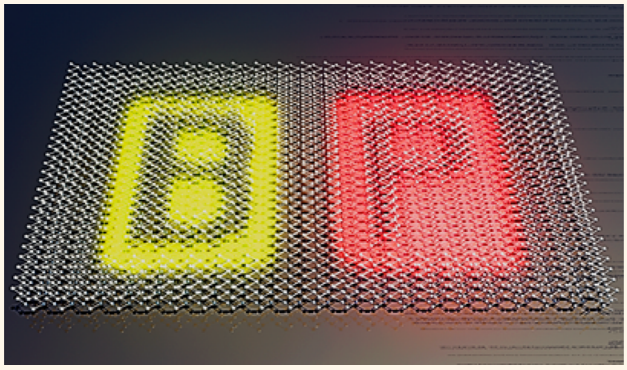

KEYWORDS: laser · phosphorene · localized oxidation · 2D material · photonics

Since the emergence of graphene,[1−4] two-dimensional (2D) materials have attracted great interest due to their extraordinary electrical, optical or photoelectrical properties.[5−8] Due to the absence of band gap in graphene, recent research efforts in 2D materials mainly focus on finding alternative 2D semiconductors. Thus, transition metal dichalcogenides (TMDs) have attracted significant attention due to their intrinsic band gap and the exciting feature of indirect to direct band gap transition as the material is thinned down to monolayer thickness.[7,9−11] The most popular TMDs include monolayer MoS_2 and WSe_2.[12−16] However, despite multiple reports that the electronic and optoelectronic devices based on monolayer TMDs have shown high on/off ratio and high responsivity, the carrier mobility of these TMDs members is still much lower than graphene.[17−19] Most recently, the rediscovery of black phosphorus (BP) demonstrated that the field-effect transistor (FET) made of few-layer BP presented both high on/off ratio and high carrier mobility.[20−23] 2D BP, with the monolayer counterpart defined as phosphorene, is the only known solid nonmetal monotypic 2D crystals besides graphene.[23−26] Although many encouraging properties including electrical, optoelectrical and thermal features of few-layer phosphorene have been demonstrated experimentally or theoretically,[20−23,27−32] there are few reports on the demonstration of control of the band gap and optical properties of these materials, especially in the visible light regime.[33] Moreover,

* Address correspondence to barbaros@nus.edu.sg, physowch@nus.edu.sg.

Received for review July 25, 2015 and accepted September 12, 2015.

Published online September 12, 2015
10.1021/acsnano.5b04623

few-layer phosphorene is prone to degradation because of various stability issues.[34−37] In this work, we demonstrate a straightforward and effective focused laser pruning approach to reduce multilayer black phosphorus (BP) to ultrathin few-layer BP under ambient condition. Naturally, shining focused laser beam onto phosphorene in ambient condition will give rise to localized oxidation. Instead of fighting this as a detrimental process, we make use of the oxidation to our advantage. Phosphorene oxides and suboxides are formed and the degree of laser-induced oxidation is controlled by the laser power. Since the band gaps of the phosphorene suboxide depend on the oxygen concentration, this simple technique is able to realize localized band gap engineering of the thin BP. The laser pruned few-layer phosphorene exhibits remarkable optical properties in visible light region. Moreover, colorful fluorescence is observed when these ultrathin few-layer phosphorene flakes are excited with light sources with different wavelength. With a scanning focused laser beam, well-defined micropatterns of few-layer phosphorene suboxide flakes with unique optical and fluorescence properties are thus fabricated. Remarkably, by monitoring the optical properties of some of these suboxide flakes, we find that the phosphorene suboxide exhibits long-term (up to 2 weeks) stability in ambient condition. Comparing against the predicted optical properties from first-principle calculations, we develop a "calibration" map in using focused laser power as a handle to tune the band gap of the BP suboxide flake. These phosphorene suboxides present an added attribute that they show high sensitivity to toxic gas such as ammonia gas. Once exposed to ammonia gas, these suboxides flakes lose their fluorescent properties. In addition, the BP suboxide flakes show their functionality in FET. The BP suboxide flakes present higher drain current modulation capacity and comparable mobility as the pristine BP flake in the FET characterizations.

RESULTS AND DISCUSSION

We exfoliated the phosphorene thin flakes from crystals of BP using the scotch tape-based approach.[1,20] The obtained flakes were transferred onto quartz substrates for further investigation. Under bright field optical microscopy, these flakes exhibit distinct and colorful images depending on the thickness of the sample. For example, Figure 1a shows an optical image of a thicker (orange) and a thinner (greenish blue) phospherene thin flake. Such a distinct different color contrasts *versus* thickness also offers the possibility to identify the layer number of phosphorene by optical images, similar to the identification of graphene[38,39] and TMDs.[40−42] Atomic Force Microscope (AFM) is well suited in measuring the thickness of these flakes. An AFM image of a typical phosphorene flake is shown in Figure 1b. The height profile indicates the thickness of the thin flake is ∼20 nm. We collected the Raman spectrum using a phosphorene thin flake and plotted the spectrum (red line) in Figure 1c. Three obvious peaks are observed at around 362.5, 439.0, and 467.5 cm^{-1}. These peaks are consistent with the Raman peaks reported for BP crystals and few-layer flakes.[22,43] They correspond to the orthorhombic structure of phosphorene and can be attributed to A_g^1, B_{2g}, and A_g^2 vibration modes, respectively.

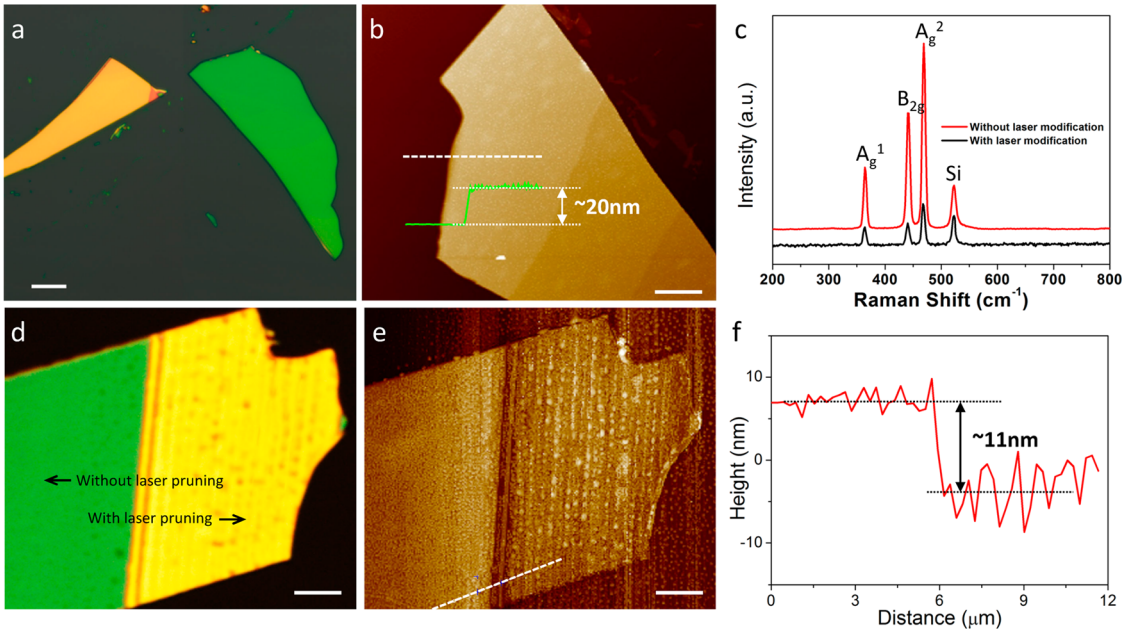

Figure 1. Structural characterizations of the BP flakes. (a) Optical images of exfoliated thicker (orange color, ∼110 nm) and thinner (green color, ∼20 nm) BP flakes. (b) AFM and (c) Raman spectrum of a BP flake. (d) Optical and (e) AFM images of a laser pruned BP flake. (f) Height profile of (e) across the pristine and laser pruning regions. Scale bar = 5 μm.

Similar to TMDs, the band structure of BP is theoretically predicted to be extremely sensitive to the number of layers.[23,28,44] Monolayer and few-layer phosphorene are expected to exhibit unique properties which are different from their bulk counterparts. Especially, phosphorene possesses a layer-dependent direct band gap. Thus, ultrathin phosphorene represents an emerging 2D material in photonics and optoelectronics with a tunable spectral response region from visible to infrared regime. Therefore, the fabrication techniques that allow one to prepare ultrathin phosphorene are highly desirable. Currently, monolayer or few-layer phosphorene are mainly produced *via* mechanical cleaving of bulk crystals. Despite the effectiveness of this method in creating ultrathin phosphorene with good quality for high performance electronic/optoelectronic device demonstration, it is worthwhile to further develop techniques to create miniaturized micropatterns form of these ultrathin phosphorene having in view future large-scale applications. Moreover, additional ways to engineer the band gap of these materials, besides thickness control, would be of great value. In our previous study, we found that a focused laser beam is an effective tool to alter the properties of nanomaterials.[13,45,46] Employing this technique on BP in ambient condition, it is possible to achieve local thinning of the BP. Hence, we refer to this method as laser pruning. Micropatterns can be readily created with a scanning focused laser beam. On top of this, when the laser thinning is carried out with the BP in ambient condition, laser-induced photochemical reactions result in localized oxidation of these BP flakes and give rise to oxidized forms of phosphorene with tunable band gap. These oxidized form of phosphorene turns out to be much more stable than their pristine counterpart. Herein, we employed the focused laser pruning technique[45] (λ = 532 nm, spot size ~1 μm) as an "on-demand" method to achieve laser-thinning and band gap engineering of multilayer BP. The multilayer BP (~30 nm) was exfoliated and deposited onto a quartz substrate. The original reflection color of pristine BP is greenish blue (Figure 1d). We subsequently subjected as-exfoliated BP flake to a focused laser beam scan with the BP flake in ambient condition. By carefully controlling the focused laser beam with a power of ~70 mW at a scanning speed of 5 μm/s in raster mode and step size of 300 nm, we constructed a uniform thinner region on the right portion of the BP (Figure 1d). Different from the laser thinning of TMDs where the optical contrast of the thinned region is identical with the layer number,[13,47] the reflection color of the laser thinned BP becomes significantly different. As shown by the optical image, the color changed to uniformly bright yellow after laser thinning. We attribute the distinct color change to the change in the thickness of the BP flake and also laser-induced localized oxidation of the BP flake. This observation supports the potential of tuning optical property of BP by this focused laser pruning technique. The resultant thinner region is further characterized using AFM and Raman spectroscopy. The AFM image in Figure 1e shows that the surface of the thinned region is rougher (with surface RMS changed from 1.02 to 4.55 nm) than the pristine region. The thickness is reduced by ~11 nm as revealed by the height profile (Figure 1f). After the laser pruning process, we repeated the Raman analysis on the laser pruned region and the resultant Raman spectrum (black line) is shown in Figure 1c. Despite the obvious reduction in intensity, the three main peaks in Raman spectrum do not show significant shift. In other words, laser thinning does not destroy the orthorhombic structure of the BP film. Besides the direct laser thinning, the focused laser beam can be employed to create micropatterns on BP flakes to miniaturize the functional devices. With the small spot size feature of the focused laser beam, well-defined micropatterns can be constructed on BP *via* programmed movement of sample stage with respect to a fixed focused laser beam. The optical image and AFM image in Figure S1 in Supporting Information demonstrate the construction of line channel patterns using the same laser power and scanning speed of the laser beam. The AFM image of the line channel (Figure S1) depicts a high spatial resolution of ~0.5 μm of focused laser pruning.

Systematic investigation is carried out to characterize the effects of focused laser pruning on BP. To ensure uniform laser modification is achieved, the scanning speed and step size were optimized at 5 μm/s and 300 nm, respectively. The uniformity of the laser thinning process is recorded and demonstrated by an *in situ* video (see Supporting Information: video captured during the laser modification process). Here, thickness engineering is controlled by carefully adjusting the laser power. The decrease in the thickness of the multilayered BP flake as a function of employed laser power is plotted in Figure 2a. The laser thinning effect is not apparent when a lower laser power (<40 mW) is used. After sufficient laser power is applied, the BP flake absorbs the light energy and converts it into heat energy, resulting in the sublimation of the top layers of the flake. The thickness is gradually thinned down further with increasing laser power. In addition to the laser thinning, photochemical process takes place and results in the oxidized form of phosphorene. When the laser power reaches 140 mW, the BP flake is thinned down to a few-layer flake. The few-layer flake is difficult to be thinned down further due to the low absorption efficiency of the few-layer phosphorene and the heat sink effect of the substrate. On the other hand, if we increase the laser power even further to 200 mW, the entire flake would be completely obliterated.

Figure 2b shows the UV–vis absorption spectra obtained from the laser pruned BP flake created with

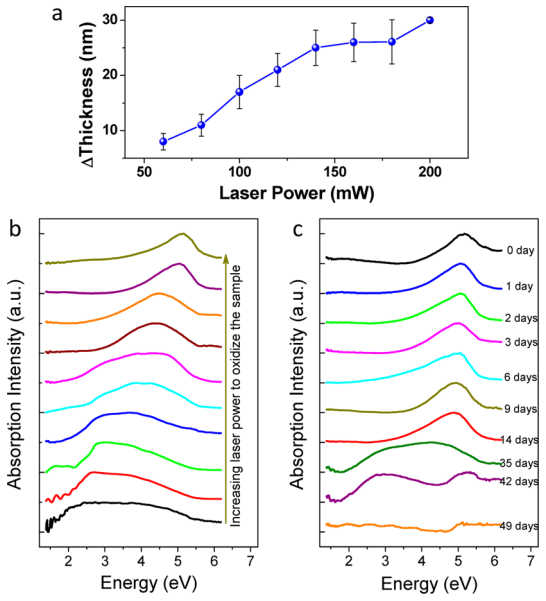

Figure 2. Influence of laser pruning to thickness and optical properties of the sample. (a) Thickness of the BP flake removed by laser pruning *versus* the power of the laser beam. (b) UV−vis spectra of the laser pruned BP flakes at increasing laser power. (c) UV−vis spectra of a laser pruned BP flake created at a laser power of 180 mW over a period of 49 days to evaluate the stability of the resultant BP flake.

increasing laser power. Evidently, the UV−vis absorption threshold is blue-shifted upon laser treatment, and the shift increases with the laser power. We attribute this observation to the laser thinning and laser-induced oxidation brought onto the BP flake once it is exposed to the focused laser beam. Both laser thinning and laser-induced oxidation of the BP result in the change in the band gap of the phosphorene. In fact, the band gap of phosphorene increases with oxidation.[48] Besides the blue-shift, other notable features of the UV−vis spectra is that pristine BP exhibits a broad spectra and the spectra become sharpened after laser treatment. The initial broad UV−vis spectra observed in pristine BP can be attributed to the wide variety of defects and disorder found on the BP flake. Laser pruning appears to have the desired advantage of pacifying such disorders and generate flake with improved and more uniform properties, albeit now we have an oxidized form of the phosphorene. The above study was repeated using another piece of sample and the results are shown in Supporting Information (Figure S2). Similar trend is reproduced. It should be emphasized that such oxidized form of the phosphorene has the added attribute that it is more stable than the exfoliated phosphorene. In Figure 2c, we follow the UV−vis adsorption spectra of a laser treated BP flake (created at a laser power of 180 mW) over a period of 49 days with the sample kept in ambient condition during these 49 days. As shown in the Figure 2c, the laser pruned BP suboxide exhibits stable UV−vis spectra for up to 14 days. This means that after the formation of phosphorene oxide, the material remained stable for up to 2 weeks. The stability of BP in air is a paramount challenge for practical applications. Our results show that instead of fighting oxidation as a detrimental process, we can make use of controlled oxidation to our advantage here to achieve band gap engineering of BP with an added advantage of prolonged stability.

To gain further insight into the detail nature of the oxidation induced by the focused laser beam, we calculate the band gap energy using hybrid functional calculations, which provide an improved description of the exchange energy and therefore a more accurate estimate of the gap value (see calculation details in Supporting Information). In this case, we made use of a model where the structures of phosphorene oxides are obtained by progressively adding oxygen to phosphorene.[48] Figure 3a shows one of the many possible phosphorene oxide structures after the incorporation of oxygen into the BP. Typically, the added oxygen can take two forms, namely dangling oxygen or bridging oxygen. Phosphorene oxides are found to be wide gap insulators. The band gap of monolayer phosphorene oxide is about 4.3 eV for 50% of incorporated oxygen, and increases smoothly with increasing oxygen concentration, reaching 8.6 eV when phosphorene is saturated with oxygen (P_2O_5). A calculation for bulk P_2O_5 shows that the band gap is nearly unchanged, unlike phosphorene for which it varies with the number of layers. However, the band gap depends on the oxygen distribution. For instance, structures where oxygen is only incorporated at the surface, occupying the dangling configuration, have smaller band gaps. Figure 3b shows the calculated band structures of phosphorene oxides with different oxygen concentrations.

It is likely that, in the present experimental conditions, there is a spatial variation of the oxygen concentration, either forming different domains or even within domains. To incorporate this variation into our model, we have considered that the number of oxygen atoms per unit cell is given by a binomial distribution with probability p. The average extinction coefficient, shown in Figure 3c, is then given by $= \Sigma_n^{10} = {}_0P_nk_n$, with $P_n = \{10!/[(10-n)!n!]\}p^n(1-p)^{10-n}$ and where k_n is the imaginary part of the refractive index for P_4O_n. For larger oxygen concentrations (higher p), the absorption threshold given by the average extinction coefficient shifts to higher energies and its spectral variation becomes broader. This corresponds to the experimental trend, although the experimentally obtained absorption spectra still shows features below 2 eV, possibly due to remaining phosphorene or defects. The extinction coefficient for the BP flake with different degree of oxidation is shown in Figure 3c.

We made a comparison between Figure 3c and Figure 2b to estimate the absorption threshold energy and the results are shown in Figure 3d. The experimental

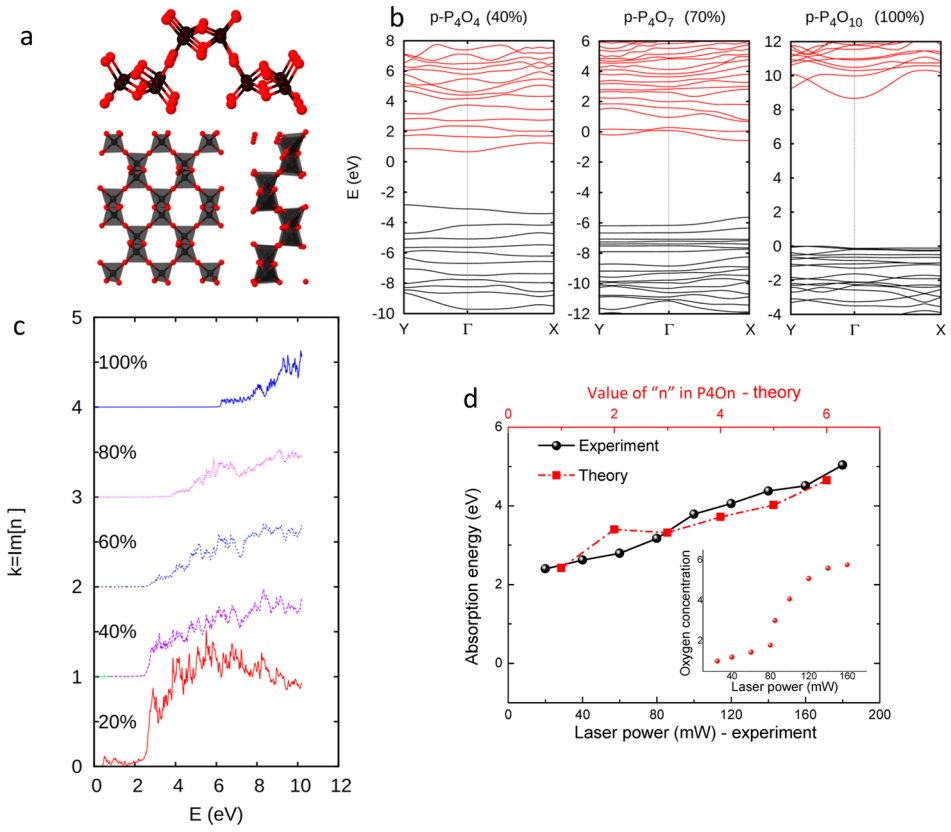

Figure 3. Optical property modification engineered by oxygen concentration. (a) Schematic diagram of a form of planar phosphorene oxide showing the dangling and bridging oxygen. (b) Band structures of selected phosphorene oxide and suboxide. (c) Imaginary part of the dielectric function for the suboxides. (d) Absorption peak energy as a function of laser power (experimental result) and oxygen concentration (theoretical result). With t he use of the chemical formula of P_4O_n, the oxygen concentration is presented as the ratio of $n/4$. Inset shows the oxygen concentration as a function of laser power. The experimental values are measured from the peak positions of the absorption spectra. The theoretical values are the direct absorption threshold energy. They are calculated by applying a rigid shift (due to inclusion of exact exchange) to the PBE band structures to correct the gap to the HSE value.

values are measured from the peak positions of the absorption spectra. The theoretical values are the direct absorption threshold energy. They are calculated by applying a rigid shift (due to inclusion of exact exchange) to the PBE band structures to correct the gap to the HSE value. While the varying factor in the case of experimental is the laser power, the handle in the case of theoretical simulation is the extent of oxidation. Thus, combining them together provides a bridge to the relation between laser power and the amount of incorporated oxygen into the BP flakes. The inset in Figure 3d is a result of this comparison and we can see that by controlling the power of the focused laser beam, we can control the oxygen content in the phosphorene suboxide and, in turn, tailor the band gap of the thin film.

When we carefully adjust the laser pruning parameters with higher laser power, ultrathin few-layer phosphorene with unique and functional optical properties is obtained after a focused laser beam thinning process. With the flexible feature of the scanning laser beam, ultrathin few-layer domains could be controllably constructed at any selected position. Figure 4a shows a bright field optical image of a few BP flakes on Si/SiO_2 substrate. Note that the BP flake at the center of the image has been laser pruned at ~160 mW and a bubble is formed due to the heating effect of the laser beam, while the rest of the laser thinned region is very thin and shows weak optical contrast. However, when viewed under a fluorescence microscope, the sample presents a unique and fascinating view. Figure 4b–e shows fluorescence microscopy (FM) images of the group of BP flakes as excited by light source with different excitation wavelengths, namely, UV light (Figure 4b, 330–380 nm), blue light (Figure 4c, 460–490 nm), green light (Figure 4d, 510–550 nm), and yellow light (Figure 4d, 550–580 nm). The most notable feature in these FM images is that only the laser pruned BP flake exhibits fluorescence signal while the other thicker BP flakes remain fluorescence inactive. More interestingly, the sample presents different fluorescent colors under different excitation with sources with different wavelengths. To elucidate the mechanism of the fluorescence property, PL spectra is carried out to quantitatively investigate the light emissions.

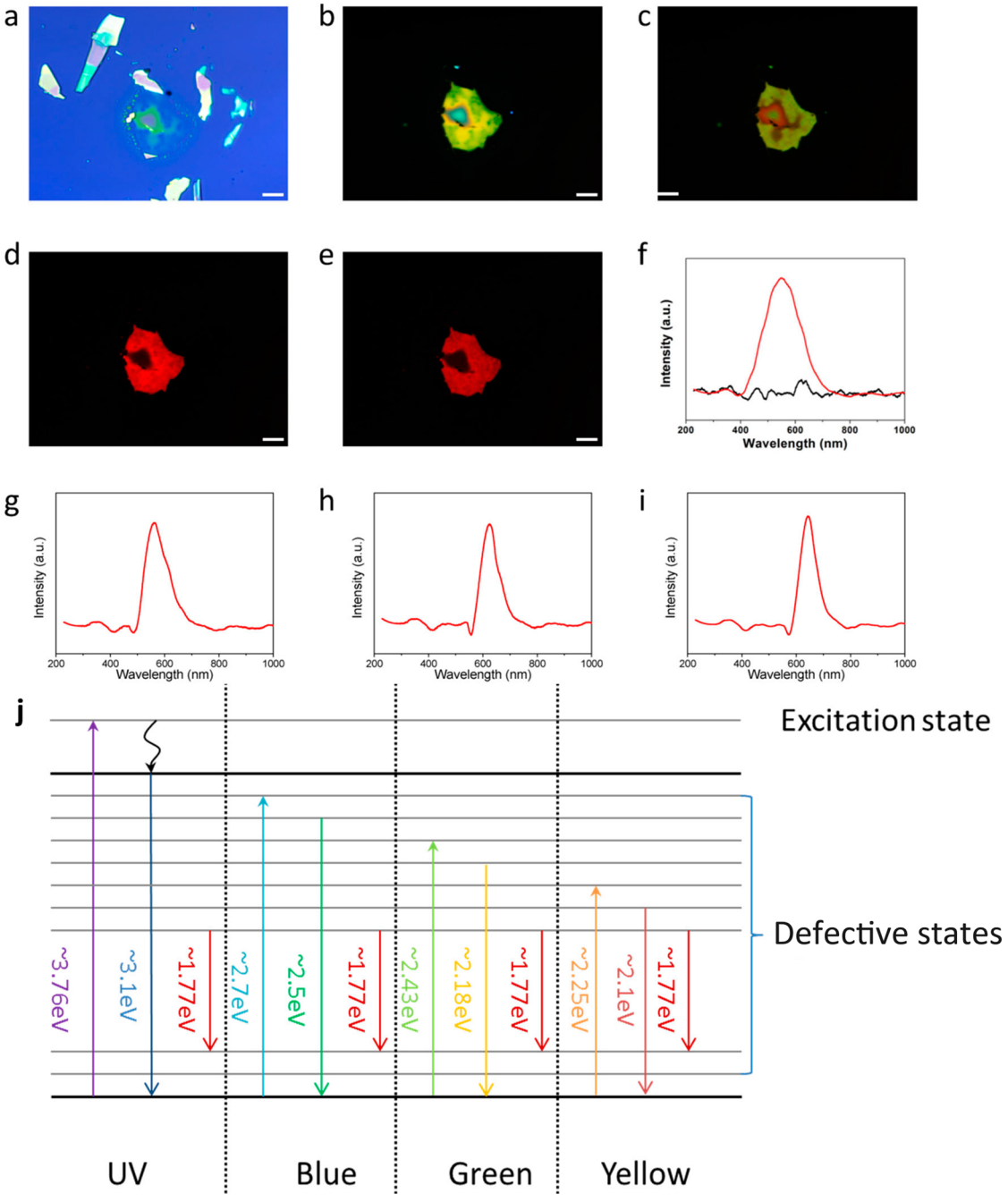

Figure 4. Fluorescence property of phosphorene oxide. (a) Bright field optical image of a few BP flakes on Si/SiO_2 substrate. Note that the BP flake at the center of the image has been laser pruned. (b–e) Fluorescence Microscopy (FM) images of the group of BP flakes as excited by light source with different excitation wavelengths. Namely, (b) UV (330–380 nm), (c) blue (460–490 nm), (d) green (510–550 nm), and (e) yellow light (550–580 nm). Scale bar = 10 μm. The most notable feature in these FM images is that only the laser pruned BP flake exhibits fluorescence signal. PL spectra of laser modified few-layer phosphorene under excitation of (f) UV (330–380 nm), (g) blue (460–490 nm), (h) green (510–550 nm), and (i) yellow light (550–580 nm), respectively. (j) Schematic illustration of the fluorescence emission processes excited under light with different wavelength.

PL spectra of laser modified few-layer phosphorene under excitation of UV (Figure 4f, 330–380 nm), blue (Figure 4g, 460–490 nm), green (Figure 4h, 510–550 nm), and yellow light (Figure 4i, 550–580 nm) confirm the PL characteristic of the laser-pruned and activated BP flake. As shown in Figure 4f, the pristine region (black curve) does not exhibit any photoactivities within the UV-NIR region when excited by UV light (330–380 nm), while the few-layer region (red curve) exhibits a strong luminescent peak centered at the visible regime. In addition, we find the photon energy of the emission light covers a broad range from ~1.77 to ~3.76 eV. The broad peak may originate from the existence of a wide variety of

Figure 5. Colorful micropatterns on phosphorene. (a) Optical images of the fabricated micropattern "NUS". (b and c) FM images of the created micropatterns showng different fluorescence colors when excited by blue (460−490 nm) and green light (510−550 nm), respectively. Scale bar = 10 μm.

defect-induced states in the gap. During the laser pruning process, defects would be introduced into the phosphorene suboxides due to the highly disruptive nature of the laser. This introduces a series of energy levels in the band gap of the phosphorene suboxides, as illustrated in Figure 4j. When the sample is excited by photons with smaller energy (changing from UV to blue/green/yellow light), the width of the PL emission peak becomes narrower. Naturally, photons with lower energy can only excite the electrons to the excitation states with lower energy (Figure 4j). Consequently, only the light with longer wavelength is emitted after recombination. As a results the FM presents greenish-yellow/red color under blue/green light excitation. The mechanism of the excitation wavelength-dependent fluorescence property is schematically illustrated in Figure 4j. These results indicate that the few-layer phosphorene is converted from nonphotoactive materials to photoactive materials after focused laser beam modification. The colorful fluorescence from these few-layer phosphorene is a promising attribute and it enhances their potential in photonic devices, such as multicolored displays.

Figure 5a−c demonstrates the application of few-layer phosphorene fabricated using laser pruning as multicolored display. As shown by the optical image (Figure 5a), the micropattern "NUS" is created onto irregularly shaped phosphorene flakes. Panels b and c of Figure 5 display the observed FM images excited by blue (460−490 nm) and green light (550−580 nm), respectively. Under fluorescence microscopy, the irregular boundary of the BP is no longer visible and only the polychrome micropatterns are observed, while the multiple colors can be easily switched *via* changing excitation wavelength.

In addition to the implementation of a multicolored display, we further find that the laser thinned few-layer phosphorene oxide can serve as all optically controlled toxic gas sensor. Figure 6a shows the optical image and colorful FM images of a laser fabricated few-layer phosphorene oxide. As described above, although a few bubbles are formed, the few-layer flake exhibits bright emission colors. Remarkably, the fluorescence is observed to show extreme sensitivity to environmental gas. We exposed the few-layer phosphorene oxide to ammonia gas (NH_3, 99.9%) for a short time (30 s). After exposure, the flake was collected and observed by FM again. The optical and FM images of the sample after NH_3 exposure is shown in Figure 6b. Notably, the exposed few-layer phosphorene oxide presents much lower optical contrast in bright field, while the bubbles become smaller. More obvious difference is revealed by the FM images. The fluorescence of the few-layer phosphorene oxide appears much weaker as compared with the state before NH_3 exposure. The quantitative change is characterized by PL spectra. As shown Figure 6c, the output intensity of the PL peak shows a significant decrease after NH_3 treatment, resulting in the fading of the fluorescence. This suggests we can use the multicolored phosphorene oxide as controlled gas sensor *via* optical display. The multicolored display can be realized by micropatterning of BP *via* focused laser pruning. Microchannel patterns are employed here to demonstrate the optical gas sensor application. The optical image in Figure 6d indicates the fabrication of well-defined microchannels. Besides the construction

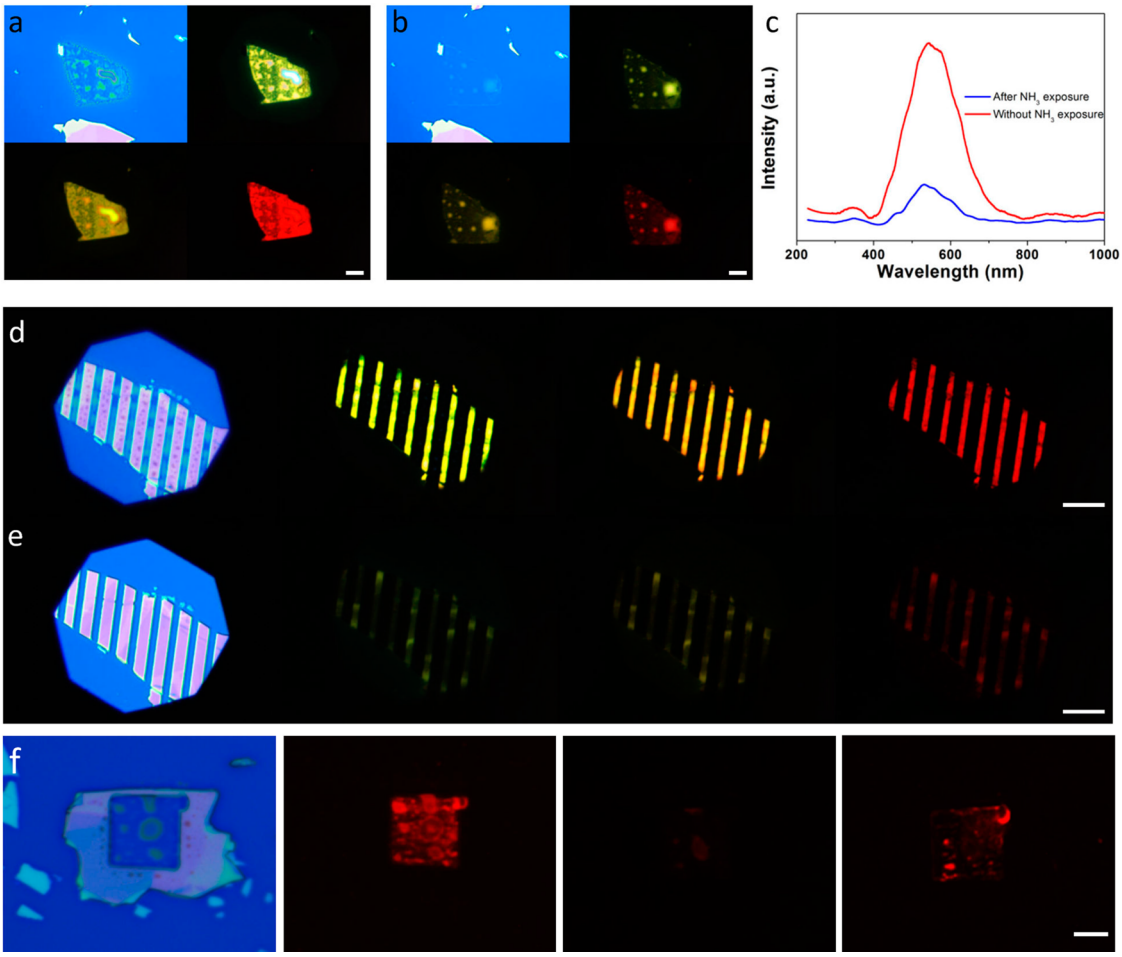

Figure 6. (a) Optical and FM images of an as-obtained few-layer phosphorene. (b) Optical and FM images of the same phosphorene flake of (a) after NH_3 exposure. (c) PL spectra before (red curve) and after (white curve) NH_3 exposure. (d) Optical and FM images of a microchannel pattern created on BP flake. (e) Optical and FM images of the same pattern of (d) after NH_3 exposure. (f) From left to right, optical image of a created phosphorene flake before NH_3 exposure, FM image of the flake before NH_3 exposure, FM image of the flake after NH_3 exposure, and FM image of the flake remodified using focused laser beam, respectively. Scale bar = 10 μm.

of the microchannels, the surfaces of the pristine regions between two channels were roughened due to the heat diffusion of the high energy laser beam. As observed by the FM images, the microchannels are colorful and multicolors are displayed. After a short exposure (~10 s) to NH_3, the FM images display a significantly different appearance. The fluorescence almost disappears and only dim colors are captured on the images (Figure 6e). By carefully comparing the optical images before and after NH_3 exposure, we found the few-layer phosphorene inside the microchannels becomes very smooth and the optical contrast is light. Even the rough surfaces of the pristine regions are smoothened after NH_3 exposure. The quenching of the fluorescence and the smoothing of the rough surface indicate the occurrence of reduction reaction of phosphorene oxide, P_xO_y, with NH_3. Accordingly, we propose the following reduction mechanism for the detection of NH_3 by laser thinned few-layer phosphorene oxide.

$$2yNH_3 + 3P_xO_y \rightarrow 3xP + yN_2 + 3yH_2O$$

Build on this attribute, the laser thinned few-layer phosphorene oxide can be designed into the component of a photonic circuit as all optically controlled gas sensors to realize the real time monitor of the toxic gas. In addition, the quenched fluorescent property of the sample after NH_3 exposure could be partially recovered when the sample is modified again using the laser pruning technique, as illustrated by the FM images (excited using yellow light) shown in Figure 6f. The optical and FM images of the flake before and after NH_3 exposure and the corresponding images of the remodified flake are shown in the Supporting Information Figure S3. This result facilitates the reusable potential of the gas sensor. On the other hand, the high sensitivity of phosphorene oxide to NH_3 facilitates NH_3 the emerging role of protecting gas which can be used to protect phosphorene from oxidization.

In addition to the optical applications of the laser thinned few-layer phosphorene, we proceed to the characterization of their field-effect behaviors to examine

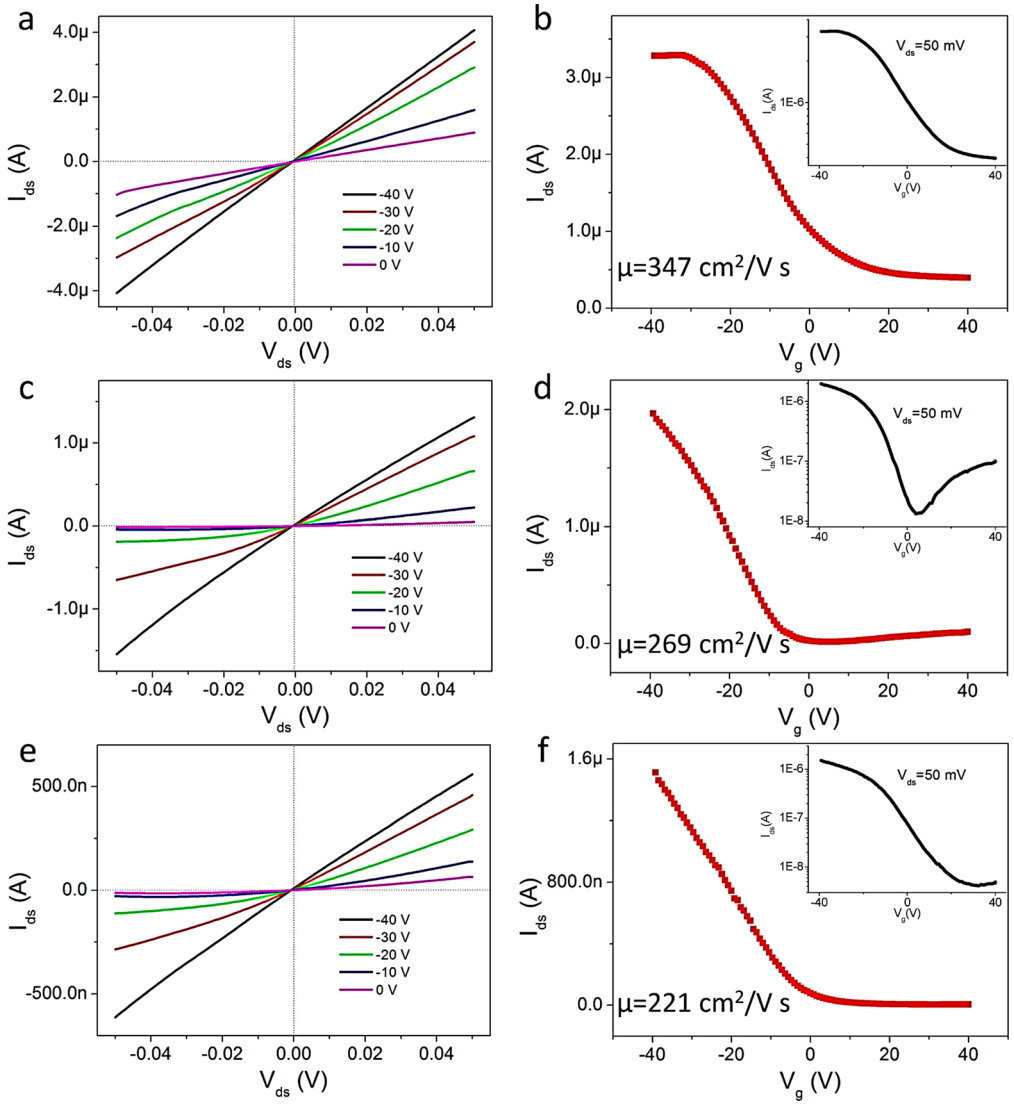

Figure 7. $I_{ds}-V_{ds}$ and $I_{ds}-V_g$ of (a and b) D1, (c and d) D2, and (e and f) D3. Insets show the $I_{ds}-V_g$ curves in the log scale.

their performance as electronic devices. We fabricated the two-terminal configuration device based on the pristine BP flakes with the thickness ~20 μm (we defined this device as D1). After the characterization, we subjected the device to a global modification by focused laser beam with laser power of ~60 mW and characterized the transport property again (this device was defined as D2). Subsequently, the device was modified further *via* focused laser with ~80 mW power to compare the effects of laser modification (this device was defined as D3). The typical $I-V$ characteristics of these devices measured at various back gate voltages from −40 to 0 V are shown in Figure 7a,c,e. Evidently, the devices show the similar gating effect behaviors, exhibiting an increasing output current with increasing gate voltages, before and after laser modification. This indicates the p-type semiconductor behavior of both pristine and modified phosphorene. The output current of the devices at V_{ds} = 50 mV were measured as a function of V_g and shown in Figure Figure 7b,d,f. The field-effect mobility was extracted from the linear region according to $\mu = g_m C_g^{-1} V_{ds}^{-1} L/W$, where $g_m = \partial I_{ds}/\partial V_g$, C_g is the gate capacitance, and L and W are the length and width of the device channel, respectively. The hole mobility is extracted to be ~347, 269, and 221 $cm^2\,V^{-1}\,s^{1-}$ for D1, D2, and D3, respectively. The mobility slightly decreases after laser modification. This is probably due to the scattering effects of the oxidation defects introduced by laser modification. The drain current modulation is extracted from the transfer characteristics in a log scale, as shown in the insets of Figure 7b,d,f. The current modulation of D1 is measured to be only ~10 which is consistent with previous reports of the devices based on the BP flakes with a thickness ~20 nm. Remarkably, the current modulation of D2 and D3 are promoted to be ~10^2 and ~10^3, after being modified and further modified by focused laser beam, respectively. The larger band gap of the laser modified few-layer phosphorene facilitates the high on/off ratio.

This result indicates that the laser modified few-layer phosphorene exhibits superior performance both in electronics and photonics.

CONCLUSION

In summary, we have reported a straightforward procedure to directly thin multilayered BP flakes down to ultrathin few-layer phosphorene suboxides by means of a focused laser pruning technique. The band gap of the phosphorene suboxides could be flexibly engineered by laser oxidation. The ultrathin few-layer phosphorene suboxides are found to be photoactive in the visible light regime. An added attribute of these ultrathin phosphorene suboxides is their extended stability when compared with as-exfoliated BP. With a scanning focused laser beam, well-defined micropatterns are achieved on BP flakes. Due to the fluorescence property of the obtained few-layer phosphorene, multicolored displays are demonstrated when the micropatterns are subjected to light excitation with different wavelength. The multicolored displays were demonstrated an optically controlled toxic gas monitor. Furthermore, the laser modified phosphorene is characterized to show higher drain current modulation than the pristine BP in the electrical applications. Our results offer 2D phosphorene suboxides as a potential functional material in both electronics and photonics.

Conflict of Interest: The authors declare no competing financial interest.

Supporting Information Available: The Supporting Information is available free of charge on the ACS Publications website at DOI: 10.1021/acsnano.5b04623.

DFT calculation details, optical and AFM images of phosphorene micropatterns, UV−vis spectra of laser pruned phosphorene at different laser powers (PDF)
Video of uniform cutting (MPG)

Acknowledgment. The authors acknowledge the National Research Foundation, Prime Minister Office, Singapore, under its Medium Sized Centre Programme. A.Z. acknowledges Prof. David F. Coker for fruitful discussions, and also an allocation of computational resources from Boston University's Office of Information Technology and Scientific Computing and Visualization. J.L. carried out the experiments. J.L. and C.H.S. wrote the manuscript. J.W. and J.Y.T. provided the material. A.C. and A.Z. carried out the theoretical simulation. H.L. helped on the absorbance measurement. Y.C. helped on the NH_3 exposure experiment. J.W. participated in the scientific discussion. The project is supervised by A.H.C.N., B.Ö., and C.H.S.

REFERENCES AND NOTES

1. Novoselov, K. S.; Geim, A. K.; Morozov, S. V.; Jiang, D.; Zhang, Y.; Dubonos, S. V.; Grigorieva, I. V.; Firsov, A. A. Electric Field Effect in Atomically Thin Carbon Films. *Science* **2004**, *306*, 666–669.
2. Novoselov, K. S.; Geim, A. K.; Morozov, S. V.; Jiang, D.; Katsnelson, M. I.; Grigorieva, I. V.; Dubonos, S. V.; Firsov, A. A. Two-dimensional gas of massless Dirac fermions in graphene. *Nature* **2005**, *438*, 197–200.
3. Zhang, Y.; Tan, Y.-W.; Stormer, H. L.; Kim, P. Experimental observation of the quantum Hall effect and Berry's phase in graphene. *Nature* **2005**, *438*, 201–204.
4. Bonaccorso, F.; Sun, Z.; Hasan, T.; Ferrari, A. C. Graphene photonics and optoelectronics. *Nat. Photonics* **2010**, *4*, 611–622.
5. Castro Neto, A. H.; Guinea, F.; Peres, N. M. R.; Novoselov, K. S.; Geim, A. K. The electronic properties of graphene. *Rev. Mod. Phys.* **2009**, *81*, 109–162.
6. Zeng, H.; Zhi, C.; Zhang, Z.; Wei, X.; Wang, X.; Guo, W.; Bando, Y.; Golberg, D. White Graphenes": Boron Nitride Nanoribbons *via* Boron Nitride Nanotube Unwrapping. *Nano Lett.* **2010**, *10*, 5049–5055.
7. Wang, Q. H.; Kalantar-Zadeh, K.; Kis, A.; Coleman, J. N.; Strano, M. S. Electronics and optoelectronics of two-dimensional transition metal dichalcogenides. *Nat. Nanotechnol.* **2012**, *7*, 699–712.
8. Schwierz, F. Graphene transistors. *Nat. Nanotechnol.* **2010**, *5*, 487–496.
9. Radisavljevic, B.; Radenovic, A.; Brivio, J.; Giacometti, V.; Kis, A. Single-layer MoS^2 transistors. *Nat. Nanotechnol.* **2011**, *6*, 147–150.
10. Mak, K. F.; Lee, C.; Hone, J.; Shan, J.; Heinz, T. F. Atomically Thin MoS_2: A New Direct-Gap Semiconductor. *Phys. Rev. Lett.* **2010**, *105*, 136805.
11. Chhowalla, M.; Shin, H. S.; Eda, G.; Li, L.-J.; Loh, K. P.; Zhang, H. The chemistry of two-dimensional layered transition metal dichalcogenide nanosheets. *Nat. Chem.* **2013**, *5*, 263–275.
12. Splendiani, A.; Sun, L.; Zhang, Y.; Li, T.; Kim, J.; Chim, C.-Y.; Galli, G.; Wang, F. Emerging Photoluminescence in Monolayer MoS_2. *Nano Lett.* **2010**, *10*, 1271–1275.
13. Lu, J.; Lu, J. H.; Liu, H.; Liu, B.; Chan, K. X.; Lin, J.; Chen, W.; Loh, K. P.; Sow, C. H. Improved Photoelectrical Properties of MoS_2 Films after Laser Micromachining. *ACS Nano* **2014**, *8*, 6334–6343.
14. Ross, J. S.; Klement, P.; Jones, A. M.; Ghimire, N. J.; Yan, J.; Mandrus, D. G.; Taniguchi, T.; Watanabe, K.; Kitamura, K.; Yao, W.; et al. Electrically tunable excitonic light-emitting diodes based on monolayer WSe_2 p−n junctions. *Nat. Nanotechnol.* **2014**, *9*, 268–272.
15. Baugher, B. W. H.; Churchill, H. O. H.; Yang, Y.; Jarillo-Herrero, P. Optoelectronic devices based on electrically tunable p-n diodes in a monolayer dichalcogenide. *Nat. Nanotechnol.* **2014**, *9*, 262–267.
16. Pospischil, A.; Furchi, M. M.; Mueller, T. Solar-energy conversion and light emission in an atomic monolayer p-n diode. *Nat. Nanotechnol.* **2014**, *9*, 257–261.
17. Fuhrer, M. S.; Hone, J. Measurement of mobility in dual-gated MoS_2 transistors. *Nat. Nanotechnol.* **2013**, *8*, 146–147.
18. Fang, H.; Chuang, S.; Chang, T. C.; Takei, K.; Takahashi, T.; Javey, A. High-Performance Single Layered WSe_2 p-FETs with Chemically Doped Contacts. *Nano Lett.* **2012**, *12*, 3788–3792.
19. Wang, H.; Yu, L.; Lee, Y.-H.; Shi, Y.; Hsu, A.; Chin, M. L.; Li, L.-J.; Dubey, M.; Kong, J.; Palacios, T. Integrated Circuits Based on Bilayer MoS_2 Transistors. *Nano Lett.* **2012**, *12*, 4674–4680.
20. Li, L.; Yu, Y.; Ye, G. J.; Ge, Q.; Ou, X.; Wu, H.; Feng, D.; Chen, X. H.; Zhang, Y. Black phosphorus field-effect transistors. *Nat. Nanotechnol.* **2014**, *9*, 372–377.
21. Liu, H.; Neal, A. T.; Zhu, Z.; Luo, Z.; Xu, X.; Tománek, D.; Ye, P. D. Phosphorene: An Unexplored 2D Semiconductor with a High Hole Mobility. *ACS Nano* **2014**, *8*, 4033–4041.
22. Xia, F.; Wang, H.; Jia, Y. Rediscovering black phosphorus as an anisotropic layered material for optoelectronics and electronics. *Nat. Commun.* **2014**, *5*, 4458.
23. Rodin, A. S.; Carvalho, A.; Castro Neto, A. H. Strain-Induced Gap Modification in Black Phosphorus. *Phys. Rev. Lett.* **2014**, *112*, 176801.
24. Maruyama, Y.; Suzuki, S.; Kobayashi, K.; Tanuma, S. Synthesis and some properties of black phosphorus single crystals. *Physica B+C* **1981**, *105*, 99–102.
25. Narita, S.; Akahama, Y.; Tsukiyama, Y.; Muro, K.; Mori, S.; Endo, S.; Taniguchi, M.; Seki, M.; Suga, S.; Mikuni, A.; et al. Electrical and optical properties of black phosphorus single crystals. *Physica B+C* **1983**, *117−118* (Part 1), 422–424.

26. Baba, M.; Nakamura, Y.; Takeda, Y.; Shibata, K.; Morita, A.; Koike, Y.; Fukase, T. Hall effect and two-dimensional electron gas in black phosphorus. *J. Phys.: Condens. Matter* **1992**, *4*, 1535.
27. Buscema, M.; Groenendijk, D. J.; Blanter, S. I.; Steele, G. A.; van der Zant, H. S. J.; Castellanos-Gomez, A. Fast and Broadband Photoresponse of Few-Layer Black Phosphorus Field-Effect Transistors. *Nano Lett.* **2014**, *14*, 3347–3352.
28. Qiao, J.; Kong, X.; Hu, Z.-X.; Yang, F.; Ji, W. High-mobility transport anisotropy and linear dichroism in few-layer black phosphorus. *Nat. Commun.* **2014**, *5*, 4475.
29. Hong, T.; Chamlagain, B.; Lin, W.; Chuang, H.-J.; Pan, M.; Zhou, Z.; Xu, Y.-Q. Polarized photocurrent response in black phosphorus field-effect transistors. *Nanoscale* **2014**, *6*, 8978–8983.
30. Han, C. Q.; Yao, M. Y.; Bai, X. X.; Miao, L.; Zhu, F.; Guan, D. D.; Wang, S.; Gao, C. L.; Liu, C.; Qian, D.; et al. Electronic structure of black phosphorus studied by angle-resolved photoemission spectroscopy. *Phys. Rev. B: Condens. Matter Mater. Phys.* **2014**, *90*, 085101.
31. Buscema, M.; Groenendijk, D. J.; Steele, G. A.; van der Zant, H. S. J.; Castellanos-Gomez, A. Photovoltaic effect in few-layer black phosphorus PN junctions defined by local electrostatic gating. *Nat. Commun.* **2014**, *5*, 4651.
32. Low, T.; Rodin, A. S.; Carvalho, A.; Jiang, Y.; Wang, H.; Xia, F.; Castro Neto, A. H. Tunable optical properties of multilayer black phosphorus thin films. *Phys. Rev. B: Condens. Matter Mater. Phys.* **2014**, *90*, 075434.
33. Wang, X.; Jones, A. M.; Seyler, K. L.; Tran, V.; Jia, Y.; Zhao, H.; Wang, H.; Yang, L.; Xu, X.; Xia, F. Highly anisotropic and robust excitons in monolayer black phosphorus. *Nat. Nanotechnol.* **2015**, *10*, 517–521.
34. Koenig, S. P.; Doganov, R. A.; Schmidt, H.; Castro Neto, A. H.; Özyilmaz, B. Electric field effect in ultrathin black phosphorus. *Appl. Phys. Lett.* **2014**, *104*, 103106.
35. Ziletti, A.; Carvalho, A.; Campbell, D. K.; Coker, D. F.; Castro Neto, A. H. Oxygen Defects in Phosphorene. *Phys. Rev. Lett.* **2015**, *114*, 046801.
36. Joshua, O. I.; Gary, A. S.; Herre, S. J. v. d. Z.; Andres, C.-G. Environmental instability of few-layer black phosphorus. *2D Mater.* **2015**, *2*, 011002.
37. Favron, A.; Gaufres, E.; Fossard, F.; Phaneuf-Lheureux, A.-L.; Tang, N. Y. W.; Levesque, P. L.; Loiseau, A.; Leonelli, R.; Francoeur, S.; Martel, R. Photooxidation and quantum confinement effects in exfoliated black phosphorus. *Nat. Mater.* **2015**, *14*, 826–832.
38. Gao, L.; Ren, W.; Li, F.; Cheng, H.-M. Total Color Difference for Rapid and Accurate Identification of Graphene. *ACS Nano* **2008**, *2*, 1625–1633.
39. Ni, Z. H.; Wang, H. M.; Kasim, J.; Fan, H. M.; Yu, T.; Wu, Y. H.; Feng, Y. P.; Shen, Z. X. Graphene Thickness Determination Using Reflection and Contrast Spectroscopy. *Nano Lett.* **2007**, *7*, 2758–2763.
40. Li, H.; Wu, J.; Huang, X.; Lu, G.; Yang, J.; Lu, X.; Xiong, Q.; Zhang, H. Rapid and Reliable Thickness Identification of Two-Dimensional Nanosheets Using Optical Microscopy. *ACS Nano* **2013**, *7*, 10344–10353.
41. Castellanos-Gomez, A.; Agraït, N.; Rubio-Bollinger, G. Optical identification of atomically thin dichalcogenide crystals. *Appl. Phys. Lett.* **2010**, *96*, 213116.
42. Ying Ying, W.; Ren, X. G.; Zhen Hua, N.; Hui, H.; Shu Peng, G.; Huan Ping, Y.; Chun Xiao, C.; Ting, Y. Thickness identification of two-dimensional materials by optical imaging. *Nanotechnology* **2012**, *23*, 495713.
43. Castellanos-Gomez, A.; Leonardo, V.; Elsa, P.; Joshua, O. I.; Narasimha-Acharya, K. L.; Sofya, I. B.; Dirk, J. G.; Michele, B.; Gary, A. S.; Alvarez, J. V.; Henny, W. Z.; et al. Isolation and characterization of few-layer black phosphorus. *2D Mater.* **2014**, *1*, 025001.
44. Tran, V.; Soklaski, R.; Liang, Y.; Yang, L. Layer-controlled band gap and anisotropic excitons in few-layer black phosphorus. *Phys. Rev. B: Condens. Matter Mater. Phys.* **2014**, *89*, 235319.
45. Lu, J.; Lim, X.; Zheng, M.; Mhaisalkar, S. G.; Sow, C.-H. Direct Laser Pruning of CdS_xSe_{1-x} Nanobelts en Route to a Multicolored Pattern with Controlled Functionalities. *ACS Nano* **2012**, *6*, 8298–8307.
46. Lu, J.; Carvalho, A.; Chan, X. K.; Liu, H.; Liu, B.; Tok, E. S.; Loh, K. P.; Castro Neto, A. H.; Sow, C. H. Atomic Healing of Defects in Transition Metal Dichalcogenides. *Nano Lett.* **2015**, *15*, 3524–3532.
47. Castellanos-Gomez, A.; Barkelid, M.; Goossens, A. M.; Calado, V. E.; van der Zant, H. S. J.; Steele, G. A. Laser-Thinning of MoS_2: On Demand Generation of a Single-Layer Semiconductor. *Nano Lett.* **2012**, *12*, 3187–3192.
48. Ziletti, A.; Carvalho, A.; Trevisanutto, P. E.; Campbell, D. K.; Coker, D. F.; Castro Neto, A. H. Phosphorene oxides: Bandgap engineering of phosphorene by oxidation. *Phys. Rev. B: Condens. Matter Mater. Phys.* **2015**, *91*, 085407.